2013 IEEE/RSJ International Conference on
Intelligent Robots and Systems (IROS)
November 3-7, 2013. Tokyo, Japan

Modeling and Analysis of Electric Field and Electrostatic Adhesion Force Generated by Interdigital Electrodes for Wall Climbing Robots

Rui Chen, Rong Liu, *Member, IEEE*, and Hua Shen

Abstract— **A model is presented for the analysis of the electric field and electrostatic adhesion force produced by interdigital electrodes. Assuming that the potential varies linearly with distance in inter-electrode gaps, the potential distribution on the electrode plane is obtained by taking the first-order Taylor series approximation. The expressions of electric field components are then derived by solving the Laplace equation for the electrical potential in each subregion. The electrostatic adhesion force is calculated using the Maxwell stress tensor formulation. The dynamic properties of the electric field and electrostatic adhesion force are assessed by evaluating the transient response of the field and force under a step in applied voltages. To verify the model developed, an experimental study is carried out in conjunction with the theoretical analysis to evaluate the adhesion performance of an electrode panel on a glass pane. A double tracked wall climbing robot is designed and tested on various wall surfaces. The limit of the approximation method of the inter-electrode potential is discussed. It is found that vacuum suction force is involved in the adhesion. The influence of this vacuum suction force on electrostatic adhesion is also discussed. The results of this work would provide support for theoretical guidelines and system optimization for the electrostatic adhesion technology applied to wall climbing robots.**

I. Introduction

Electrostatic adhesion technology has broad application prospects on wall climbing robots for its unique characteristics over other types of adhesion technologies. It uses a compliant electrode panel with shaped electrodes designed to create electrostatic adhesion force between the wall surface and the robot. Wall climbing robots based on this technology perform well on a wide variety of materials, both conductive and nonconductive, including surfaces such as concrete, wood, steel, glass, drywall, and brick [1], [2], [3]. Even though practical application of electrostatic adhesion technology to wall climbing robots has been investigated in recent years, the theoretical study of this technology is far from mature. Little work has been published on the calculation of electric field and electrostatic adhesion force, especially the dynamic properties of them. Design and control of a wall climbing robot based on electrostatic adhesion technology are mainly dependent on empirical analysis or repeated tests.

Generally, electrostatic adhesion force used for wall climbing robots is obtained by exerting the voltages to the shaped electrodes. Among many different types of electrodes examined, interdigital electrodes show many good features [4]. The interdigital electrodes are similar, consisting of a large number of thin parallel bar electrodes fabricated on a flat substrate. As we know, the electrostatic force is directly dependent on the electric field. Thus knowledge of the electric field and the electrostatic force generated by the interdigital electrodes is essential for improving the work performance of wall climbing robots.

However, due to the non-uniformity of the electric field generated by the interdigital electrodes, modeling and analysis of the electric field (and as a result the electrostatic adhesion force) is not an easy work. So far, the electric field for an interdigital electrode has been solved mainly by numerical methods, such as point charge [5], charge density [6], finite element [7], as well as analytical approximation based on Green's functions [8], point matching [9] and Fourier series [10]. All of the numerical methods suffer from the problem of intensive computation and low accuracy, and can-not provide enough theoretical guidance for the actual application, such as the optimization of the proposed electrode configurations. An analytical approach to field determinations is desirable to provide more rapid and accurate solutions. However, some of the existing methods mainly aim at some specific application areas, such as dielectrophoresis and electrostatic suspension [11], where the electrode arrays are usually placed in a single homogeneous medium. In addition, there are few literatures concerning the dynamic properties of the electric field and the electrostatic adhesion force.

The aim of this paper is to develop an analytical model for the electric field and electrostatic adhesion force generated by the interdigital electrodes. A typical adhesion system consisting of an electrode panel and a dielectric plate positioned below the electrode panel is considered. The electric field problem involves solving the Laplace equations with the boundary conditions taken into account. Based on this model, field and force dynamics are investigated as a function of structure parameters of the electrode panel and electrical parameters of the system. Experiment is carried out to evaluate the adhesion performance of the electrode panel on a glass pane, and the experimental results verify the correctness of the theoretical model. Based on the theoretical model, a double tracked wall climbing robot prototype is designed and the performance of the robot on various wall surfaces is tested. Finally, we discuss the limit of the approximation method of the inter-electrode potential. The influence of vacuum suction force on the adhesion system is also discussed.

All authors are with the Robotics Institute, School of Mechanical Engineering and Automation, Beihang University, Beijing, 100191, People's Republic of China (phone: +86-010-82314554; fax: +86-010-82314554; e-mail: buaacr@ 163.com).

II. THEORETICAL MODELING

A. Physical Model

A basic model that can adequately describe the performance of the interdigital electrodes is depicted in Fig. 1. In this model, the electrode structure consists of two interpenetrating comb electrodes, each having a number of fingers of length L. Time-varying electric potentials $V_{\mathrm{p}}(t)$ and $V_{\mathrm{n}}(t)$ are exerted on the electrodes. The electrodes are of width $2w$ and are spaced equidistantly with pitch p. The electrodes, made of copper in general, are deposited on a polyimide film with a thickness of d_2. Another polyimide film of thickness d_1 is covered on the electrodes for electric insulation. Both of the two polyimide films have uniform permittivity ε_{p} and volume conductivity σ_{p}. The polyimide films and the copper electrodes sandwiched between the two films constitute an electrode panel, which is used to generate electric field and force under a voltage excitation. Positioned below the electrode panel is a dielectric plate with the thickness being d_4, uniform permittivity being ε_{d} and volume conductivity being σ_{d}. Given the roughness of the dielectric surface, a simplified thin air layer with a thickness of d_3 is taken into account between the electrode panel and the dielectric plate.

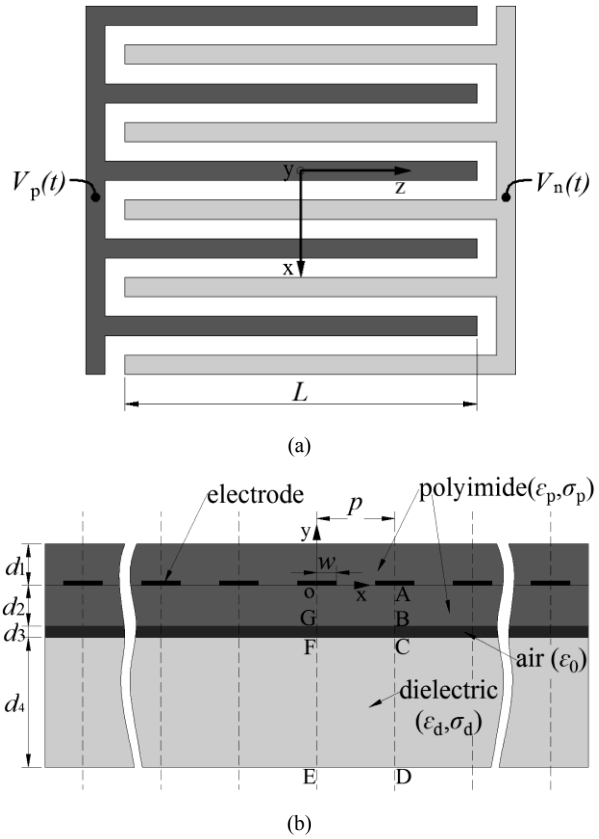

Figure 1. (a) Layout of interdigital electrodes. (b) Cross-section of the adhesion model.

B. Basic equations and assumptions

Since currents are varying at a sufficiently small rate, Maxwell's equations can be reduced to the quasi-electrostatic form [12]:

$$\boldsymbol{E} = -\nabla\phi, \tag{1}$$

$$\nabla\cdot\boldsymbol{D} = \rho, \tag{2}$$

$$\nabla\cdot\boldsymbol{J} + \frac{\partial\rho}{\partial t} = 0, \tag{3}$$

where $\boldsymbol{E}$ is the electric field, $\boldsymbol{D}$ is the electric flux density or the displacement vector, ρ is the free charge density, and $\boldsymbol{J}$ is the conduction current. For a homogeneous linear dielectric with permittivity ε and conductivity σ, $\boldsymbol{D} = \varepsilon\boldsymbol{E}$ and $\boldsymbol{J} = \sigma\boldsymbol{E}$.

Given the particular interdigital electrodes, some simplifications and assumptions can be made. Since electric field is generated mainly between neighbouring comb fingers, we simplify the comb electrodes into a planar array of parallel strip electrodes without consideration of the effect of the root segments of the electrodes. As the length of electrodes (L) is much larger than the width of them ($2w$) and the thickness of air layer (d_3), the edge effect along the length direction can be ignored. In addition, the electric field along the length direction is uniform, so we can transform this 3D problem into a 2D one by taking the cross-section of the electrode panel into consideration. Due to the periodicity of the electrode structure, we can choose one period as the research object, which is the region of $0 \le x \le p$. From Fig. 1, it is evident that the electrode structure is even symmetry along the centerlines, so the problem space required for the correct solution to the electric field problem can be reduced to the region bounded by OADE.

Due to the presence of the stratified dielectric mediums, the electric field exhibits discontinuities on boundaries GB and FC. For this reason, the problem space is divided into three rectangular piece-wise uniform subregions: OABG, GBCF and FCDE. In the following, we shall denote these regions as subregions 1, 2, and 3. In each subregion, the potential is a solution of Laplace equation, which in an isotropic medium, assumes the form:

$$\frac{\partial^2\phi(x,y,t)}{\partial x^2} + \frac{\partial^2\phi(x,y,t)}{\partial y^2} = 0, \tag{4}$$

where $\phi(x,y,t)$ is the spatial time-varying potential distribution. By using the method of separation of variables [12], a general solution to (4) can be derived as a combination of $\phi_{\lambda=0}(x,y,t)$ and $\phi_{\lambda\neq0}(x,y,t)$:

$$\begin{aligned}\phi(x,y,t) &= \phi_{\lambda=0}(x,y,t) + \phi_{\lambda\neq0}(x,y,t)\\ &= [A(t)x + B(t)][C(t)y + D(t)]\\ &\quad + [E(t)\sin(\lambda x) + F(t)\cos(\lambda x)]\\ &\quad \times [G(t)\sinh(\lambda y) + H(t)\cosh(\lambda y)],\end{aligned} \tag{5}$$

where λ is the separation constant. Independent particular solutions $\phi_{\lambda=0}(x,y,t)$ and $\phi_{\lambda\neq 0}(x,y,t)$ correspond to the two separate cases $\lambda = 0$ and $\lambda \neq 0$, respectively.

The arbitrary time-varying coefficients $A(t)$, $B(t)$, $C(t)$, $D(t)$, $E(t)$, $F(t)$, $G(t)$, $H(t)$, and the separation constant λ are determined such that $\phi(x,y,t)$ satisfies the boundary conditions.

C. Boundary conditions

The three subregions which make up the problem space have in common that the potential in each subregion is finite and symmetry on the planes $x = 0$ and $x = p$, therefore, the Neumann-type boundary conditions should be followed:

$$\frac{\partial\phi(0,y,t)}{\partial x} = 0, \quad \frac{\partial\phi(p,y,t)}{\partial x} = 0, \quad -(d_2+d_3+d_4) \le y \le 0. \tag{6}$$

Since the electrodes are much thinner than their width, we ignore the thickness so that the potential on the electrodes is specified at $y = 0$. The potential distribution on the positive and negative electrodes is specifically described by the applied voltages $V_{\mathrm{p}}(t)$ and $V_{\mathrm{n}}(t)$. However, this is not a complete boundary condition of the potential distribution on the entire electrode plane because the electrodes do not form a closed surface and the potentials in the inter-electrode gap are unknown. Here for clarity and convenience, we will take the first-order Taylor series approximation by assuming that the potential varies linearly with distance in the electrode gaps. Thus the boundary conditions for our model are given by:

$$\phi(x,0,t) = \begin{cases} V_{\mathrm{p}}(t) & 0 \le x \le w \\ \dfrac{V_{\mathrm{p}}(t)+V_{\mathrm{n}}(t)}{2} + [V_{\mathrm{n}}(t)-V_{\mathrm{p}}(t)]\dfrac{x-p/2}{p-2w} & w \le x \le p-w \\ V_{\mathrm{n}}(t) & p-w \le x \le p \end{cases}. \tag{7}$$

The analytical expression for the potential on the boundary plane $y = 0$ is piecewise smooth in the interval $0 \le x \le p$. By using Fourier series expansion, we can obtain an expression that is continuously smooth in the interval $0 \le x \le p$, which is convenient for subsequent discussions. As this potential is an even function with respect to the y axis, only the cosine terms are retained in its Fourier series representation:

$$\phi(x,0,t) = \frac{V_{\mathrm{p}}(t)+V_{\mathrm{n}}(t)}{2} + \frac{2[V_{\mathrm{n}}(t)-V_{\mathrm{p}}(t)]}{\pi^2(1-2w/p)} \times \sum_{n=1}^{\infty}\frac{1}{n^2}[\cos(n\pi - \frac{n\pi w}{p}) - \cos(\frac{n\pi w}{p})]\cos(\frac{n\pi x}{p}) \quad 0 \le x \le p. \tag{8}$$

Boundary conditions related to the three rectangular piece-wise uniform subregions can be divided into two parts, which are with respect to the two dielectric interfaces. The boundary conditions representing the irrotational condition of the electric field can be given by:

$$\begin{aligned} \boldsymbol{n}\times(\boldsymbol{E}_1-\boldsymbol{E}_2) &= 0, \quad y = -d_2 \\ \boldsymbol{n}\times(\boldsymbol{E}_2-\boldsymbol{E}_3) &= 0, \quad y = -(d_2+d_3). \end{aligned} \tag{9}$$

The boundary conditions associated with the charge conservation law (or the continuity of current) at the two dielectric interfaces can be written as [13]:

$$\begin{aligned} \frac{\partial}{\partial t}\boldsymbol{n}\cdot(\varepsilon_{\mathrm{p}}\boldsymbol{E}_1-\varepsilon_0\boldsymbol{E}_2)+\boldsymbol{n}\cdot(\sigma_{\mathrm{p}}\boldsymbol{E}_1) &= 0, \ y = -d_2 \\ \frac{\partial}{\partial t}\boldsymbol{n}\cdot(\varepsilon_0\boldsymbol{E}_2-\varepsilon_{\mathrm{d}}\boldsymbol{E}_3)-\boldsymbol{n}\cdot(\sigma_{\mathrm{d}}\boldsymbol{E}_3) &= 0, \ y = -(d_2+d_3) \end{aligned} \tag{10}$$

where $\boldsymbol{n}$ is the unit vector of the y axis, $\boldsymbol{E}_1$, $\boldsymbol{E}_2$ and $\boldsymbol{E}_3$ are the electric field in subregions 1, 2 and 3, respectively.

In general, since the thickness of the dielectric plate is much larger than that of the polyimide film and the air layer ($d_4 >> d_2, d_4 >> d_3$), d_4 is usually treated as infinity for reasonable simplification. The last boundary condition expresses that the potential decays to zero when y approaches infinity, that is:

$$\lim_{y\to-\infty}\phi(x,y,t) = 0. \tag{11}$$

Equations (6), (8), (9), (10) and (11) constitute the complete set of boundary conditions necessary to solve the posed boundary problem.

D. Electric field and electrostatic adhesion force

Each of the electric field components in subregions 1, 2, 3 can be derived from (1) after we obtain the potential distributions in the three regions. In order to get the potential distributions in the three subregions, we need to solve the Laplace equation for each region by considering the general solution and boundary conditions. Here, we take the Laplace transforms of the time functions to circumvent the computational difficulty created by the presence of the time derivatives of field solutions in the boundary conditions (10). The Laplace transforms of time domain functions are denoted by replacing the time variable t with the complex variable s. Therefore, the electric field components in each subregion are expressed as the product between the voltage difference $V_{\nabla}(s)$ and the sum of an infinite series of rational, second-order transfer functions, as follows:

$$E_{r,x}(x,y,s) = \frac{\pi}{p}V_{\nabla}(s)\sum_{n=1}^{\infty}n\gamma(n)\sin(\frac{n\pi x}{p}) \times \frac{a^r_{2,x}(n,y)s^2 + a^r_{1,x}(n,y)s + a^r_{0,x}(n,y)}{b_2(n)s^2 + b_1(n)s + b_0(n)},$$

$$E_{r,y}(x,y,s) = -\frac{\pi}{p} V_{\nabla}(s) \sum_{n=1}^{\infty} n\gamma(n) \cos(\frac{n\pi x}{p}) \times \frac{a_{2,y}^{r}(n,y)s^2 + a_{1,y}^{r}(n,y)s + a_{0,y}^{r}(n,y)}{b_2(n)s^2 + b_1(n)s + b_0(n)}, \quad (12)$$

where $r = 1, 2, 3$ indicate the three subregions and

$$V_{\nabla}(s) = V_{\mathrm{p}}(s) - V_{\mathrm{n}}(s),$$

$$\gamma(n) = \begin{cases} 0 & n = \text{even} \\ \dfrac{4\cos(n\pi w/p)}{n^2\pi^2(1-2w/p)} & n = \text{odd} \end{cases}.$$

A dynamic relation, which includes a time-varying function, exists between the applied electrode voltages and electrostatic adhesion force due to the resistivity of the dielectric and the delayed polarization. In this work, the field and force dynamics are assessed by evaluating the transient response of the field and force under a step in applied voltages, and these are in accord with the actual adhesion process where the voltages exerted to the electrodes may actually behave like a step input. Let us define the step voltages as:

$$\begin{cases} V_{\mathrm{p}}(t) = 0, & \text{if } t \le 0 \\ V_{\mathrm{p}}(t) = V_{\mathrm{p}}, & \text{if } t > 0 \end{cases} \text{ and } \begin{cases} V_{\mathrm{n}}(t) = 0, & \text{if } t \le 0 \\ V_{\mathrm{n}}(t) = V_{\mathrm{n}}, & \text{if } t > 0 \end{cases}. \quad (13)$$

The Laplace transforms of these step voltages are given by $V_{\mathrm{p}}(s) = V_{\mathrm{p}}/s$ and $V_{\mathrm{n}}(s) = V_{\mathrm{n}}/s$. The time domain electric filed components can then be obtained straightforwardly by applying the inverse Laplace transform to (12).

In this work, the electrostatic adhesion force exerted on the dielectric plate can be calculated by using the Maxwell stress tensor formulation. The net ith force component on a dielectric medium is obtained by integrating the Maxwell stress tensor $\boldsymbol{T}_{ij}$ over the enclosing surface S [14],

$$F_i = \varepsilon_0 \oint_s (T_{ij} n_j) dA = \varepsilon_0 \oint_s [(E_i E_j - \frac{1}{2}\delta_{ij} E_k E_k) n_j] dA, \quad (14)$$

where the Einstein convention has been used for vector indices and δ_{ij} is the Kronecker delta. In addition, the integration in (14) should take place over the outer boundary of the enclosing surface S. Since $d_4 >> d_2, d_4 >> d_3$ and d_4 is usually treated as infinity for reasonable simplification, the potential on the lower surface of the dielectric plate decays to zero, and the electric field decays to zero as well. This implies that only the electric field solution in subregion 2 is required in the integration, so the electrostatic adhesion force exerted on the dielectric plate of one period can be written as:

$$F = \frac{\varepsilon_0 L}{2} \int_0^p [E_{2,y}^2(x,y,t) - E_{2,x}^2(x,y,t)] dx. \quad (15)$$

III. Model Verification and Analysis.

To verify the model developed, adhesion performance of an electrode panel on a glass pane is evaluated. The electrode panel with a pair of interdigital electrodes as shown in Fig. 2 is made from a flexible etched printed circuit board by removing copper films. The base of the panel is a polyimide film with $d_2 = 50\,\mu$m. Interdigital electrodes made from the copper film are deposited on the polyimide base, which are then covered by another polyimide film with $d_1 = 50\,\mu$m. The bulk electrical properties of the polyimide films are $\varepsilon_{\mathrm{p}} = 3.4\varepsilon_0$ and $\sigma_{\mathrm{p}} = 10^{-17}$ S/cm, where $\varepsilon_0 = 8.85 \times 10^{-12}$ F/m is the permittivity of vacuum. The width of the electrode and the space between neighbouring electrodes are both 1 mm, and the length of the electrode is $L = 300$ mm. The total area of the electrode panel is $A = 300\text{ mm} \times 200\text{ mm}$. The glass pane has a thickness (d_4) of 5 mm, while the thickness of the air layer between the electrode panel and the glass pane due to the influence of roughness is assumed to be $d_3 = 20\,\mu$m. The bulk electrical properties of the glass pane are given by $\varepsilon_{\mathrm{d}} = 3.5\varepsilon_0$ and $\sigma_{\mathrm{d}} = 10^{-13}$ S/cm, and the applied step voltages are $V_{\mathrm{p}} = 800$ V and $V_{\mathrm{n}} = -800$ V.

A. Numerical Computation and Experiment

Since the series expansion of the field components are summations over an infinite number of terms, they need to be truncated by considering reasonable accuracy of the model and complexity of the computation. Based on the above considerations, the choice of the summation index $n_{total} = 31$ is verified to lead to a rapid convergence of the sum and the dynamic properties of field and adhesion force can also be demonstrated well. The numerical results are carried out by using the numerical software package MATLAB. In addition, experiment work of the electrode panel on the glass pane is conducted, and experimental results and theoretical consequences are both presented to verify the model.

Fig. 3 depicts the time histories of the step response of the field components on the boundary $y = -(d_2 + d_3)$ in subregion 2 [Fig. 3(a) and Fig. 3(b)] and on the boundary $y = -(d_2 + d_3 + d_4)$ in subregion 3 [Fig. 3(c) and Fig. 3(d)]. These plots show that all field components except for $E_{2,y}(x,y,t)$ decay to zero as the time increases. We also notice that the field components on the boundary $y = -(d_2 + d_3 + d_4)$ are much smaller than that on the boundary $y = -(d_2 + d_3)$, which proves that ignoring the influence of field components on the boundary $y = -(d_2 + d_3 + d_4)$ in the integration when calculating the adhesion force is reasonable. Fig. 4 depicts the time histories of the electrostatic adhesion force exerted on the glass pane. Both the experimental data and theoretical data demonstrate that it needs almost 100 s for the adhesion force to increase gradually to a steady value. The discrepancy between the presented experimental data and the theoretical results mainly results from two aspects: (a) the linear approximation of the potential distribution in the inter electrode gap, which results in the inherent error of the model; (b) the influence of the vacuum suction force, which will be discussed in the following section.

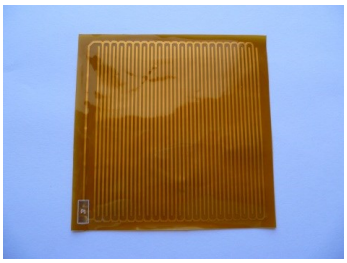

Figure 2. An electrode panel with a pair of interdigital electrodes.

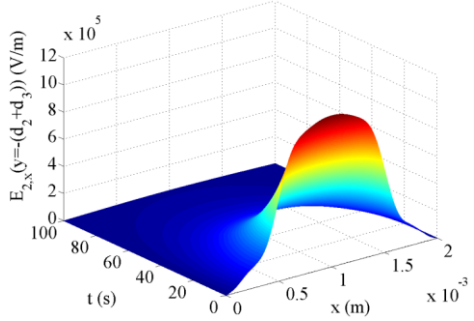

(a)

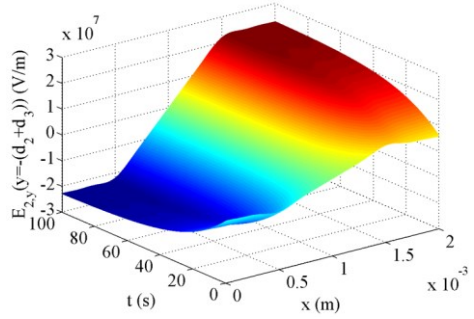

(b)

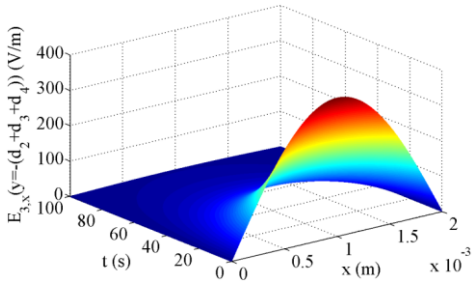

(c)

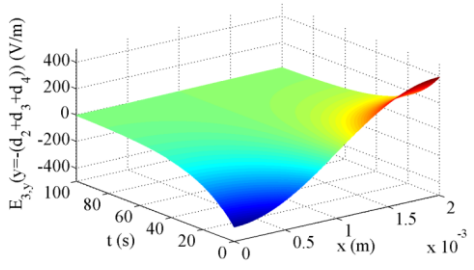

(d)

Figure 3. The step response of the electric field components as a function of time (t) and distance (x) along the boundary $y=-(d_2+d_3)$ in subregion 2 [(a) and (b)] and $y=-(d_2+d_3+d_4)$ in subregion 3 [(c) and (d)].

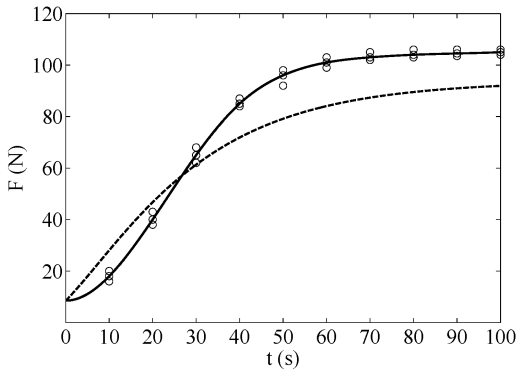

Figure 4. Time histories of the electrostatic adhesion force exerted on the glass pane. Theoretical results (---) and experimental results (—).

B. Prototype Wall Climbing Robot Using Electrostatic Adhesion Force

1) Design

Based on the theoretical model above, a double tracked wall climbing robot has been designed as shown in Fig. 5. Two flexible electrode panels not only are used to generate electrostatic adhesion force, but also play the role of being the travelling mechanism of the robot. Two tails are employed in this robot structure to improve the ability of anti-peeling of the robot. The robot is driven using two DC motors powered by three lithium batteries in series. The batteries also directly power the electrode panel through the use of a commercially available DC-DC high voltage converter, which can output several thousand volts. In order to simplify the robot prototype, we utilize remote control to control the movement of the robot.

Figure 5. A double tracked wall climbing robot prototype.

TABLE I. MAIN PERFORMANCE PARAMETERS OF THE ROBOT PROTOTYPE

Self-weight	700 g
Size	360 mm * 360 mm
Maximum velocity	5cm/s
Turning radius	⩾0.5 m
Power supply voltage	12 V
Adhesion voltage	3000 V
Maximum holding force	20 N
Power consumption	3 W

2) Test

We test the climbing performance of the robot prototype on various wall surfaces. The experiment results are satisfactory, which verifies the feasibility of electrostatic adhesion technology for wall climbing robots and the rationality of the theoretical model and computation method proposed in this paper. The robot can achieve forward and backward movements freely on different wall surfaces, meanwhile, it can also turn on the wall with a turning radius that is not too small. Due to the charge relaxation mechanism, the maximal velocity of the robot is limited to approximately 5cm/s. The main performance parameters of the robot prototype are given in Table I.

IV. Discussion

A. Approximation of The Inter-electrode potential

In the physical model given above, for clarity and convenience, we take the first-order Taylor series approximation, assuming that the potential varies linearly with distance in the electrode gaps. However, this linear approximation of the field in the inter-electrode gap, generally leading to lower peak values of the field at the electrode edges, consequently results in the existing discrepancy between presented experimental results and theoretical results. A third or higher order approximation for the electrostatic potential in the inter-electrode gap can further improve the model accuracy over the linear approximation.

B. Influence of Vacuum Suction Force

From the observation of the performance of the electrode panel on the glass pane, it is speculated that vacuum suction force, such as that in a suction cup, is also involved in adhesion. Due to the flexibility of the electrode panel, the small gap with low air pressure is generated, resulting in the vacuum suction force when electrostatic adhesion is activated. At the initial phase of the adhesion, experimental data are smaller than the theoretical data because the contact between the electrode panel and the glass pane is not close enough, which certainly reduces the adhesion force. As the adhesion force gradually increases with time, the electrode panel contact more closely with the glass pane. Meanwhile, the air beneath the electrode panel is squeezed out and the negative pressure environment is formed, resulting in the vacuum suction force exerted on the electrode panel. The theoretical data are larger than the experimental data when the adhesion reaches a steady value at the final phase because of the influence of the vacuum suction force.

V. Conclusion

This paper has introduced an analytical model to analyze the electric field and electrostatic adhesion force generated by interdigital electrode arrays. The expressions of electric field components are derived by solving the Laplace equation for the electrical potential in each subregion. The electrostatic adhesion force is calculated by using the Maxwell stress tensor formulation. Experiments are carried out to verify the model by evaluating the adhesion performance of an electrode panel on a glass pane. A double tracked wall climbing robot prototype using electrostatic adhesion force is designed, and it performs very well on various wall surfaces. We find a relatively good agreement between theory and experiment. A third or higher order approximation for the electrostatic potential in the inter-electrode gap can further improve the model accuracy over the linear approximation. In addition, we find that vacuum suction force is also involved in the adhesion. The outcome of this work can provide support for theoretical guidelines and system optimization for wall climbing robots based on electrostatic adhesion technology. Further study is needed to analyze the important factors which influence the electrostatic adhesion problem, especially the dynamic response speed of the adhesion force. Another area for future investigation can be focused on the mathematical modeling of the surface roughness instead of the simplified uniform air layer in this paper.

References

[1] A. Yamamoto, T. Nakashima and T. Higuchi, "Wall climbing mechanisms using electrostatic attraction generated by flexible electrodes," *Int. Symp. on Micro-Nano Mechatronics and Human Science*, Nagoya, 2007, pp. 389–94.

[2] H. Prahlad, R. Pelrine, S. Stanford, J. Marlow and R. Kornbluh, "Electroadhesive robots—Wall climbing robots enabled by a novel, robust, and electrically controllable adhesion technology," *IEEE International Conference on Robotics and Automation*, Pasadena, CA, USA, May 19–23, 2008, pp. 3028-3033.

[3] R. E. Pelrine, H. Prahlad, J. S. Eckerle, R. D. Kornbluh and S. Stanford, "Electroadhesive devices," U.S. Patent 0 120 544 A1, May 17, 2012.

[4] K. Yatsuzuka, F. Hatakeyama, K. Asano and S. Aonuma, "Fudamental characteristics of electrostatic wafer chuck with insulating sealant," *IEEE Trans. Ind. Appl.* vol. 36, no. 2, pp. 510–516, Apr. 2000.

[5] T. Schnelle, R. Hagedorn, G. Fuhr, S. Fiedler and T. Muller, "Three-dimensional electric field traps for manipulation of cells—calculation and experimental verification," *Biochim. Biophys. Acta*, vol. 1157, no. 3, pp. 127–40, July 1993.

[6] X. B. Wang, Y. Huang, J. P. H. Burt, G. H. Markx and R. Pethig, "selective dielectrophoretic confinement of bioparticles in potential energy wells," *J. Phys. D: Appl. Phys.*, vol. 26, no. 8, pp. 1278–1285, Aug. 1993.

[7] N. G. Green, A. Ramos and H. Morgan, "Numerical solution of the dielectrophoretic and travelling wave forces for interdigitated electrode arrays using the finite element method," *J. Electrost.*, vol. 56, pp. 235–254, 2002.

[8] X. J. Wang, X. B. Wang, F. F. Becker and P. R. C. Gascoyne, "A theoretical method of electrical field analysis for dielectrophoretic electrode arrays using Green's theorem," *J. Phys. D: Appl. Phys.*, vol. 29, no. 2, pp. 1649–1660, June 1996.

[9] D. Marcuse, "Electrostatic field of coplanar lines computed with the point matching method," *IEEE J. Quantum Electron.*, vol. 25, no. 5, pp. 939–947, May 1989.

[10] H. Morgan, A. G. Izquierdo, D. Bakewell, N. G. Green and A. Romos, "The dielectrophoretic and travelling wave forces generated by interdigitated electrode arrays: analytical solution using Fourier series," *J. Phys. D: Appl. Phys.*, vol. 34, no.10, pp. 1553–61, May 2001.

[11] S. J. Woo and T. Higuchi, "Electric field and force modeling for electrostatic levitation of lossy dielectric plates," *J. Appl. Phys.*, vol. 108, no. 10, Nov. 2010.

[12] H. A. Haus and J. R. Melcher, *Electromagnetic Fields and Energy*, NJ: Prentice Hall, 1989.

[13] Z. W. Zhang, "Modeling and analysis of electrostatic force for robot handling of fabric materials," *IEEE-ASME Trans. Mechatron.*, vol. 4, no. 1, pp. 39–49, Mar. 1999.

[14] R Melcher, *Continuum Electromechanics*, Cambridge MA: MIT Press, 1981.